Advanced Composites and Hybrid Materials
https://doi.org/10.1007/s42114-021-00255-8

ORIGINAL RESEARCH

Ultrasonic-assisted soldering for graphite films as heat sinks with durably superior heat dissipating efficiency

Huaqiang Fu[1] · Yong Xiao[1] · Peng Li[2] · Wei Qian[2] · Dan Li[1] · Xin Zhao[2] · Daping He[2,3]

Received: 28 February 2021 / Revised: 29 March 2021 / Accepted: 8 April 2021
© The Author(s), under exclusive licence to Springer Nature Switzerland AG 2021

Abstract

Graphite film (GF) is considered as an unrivaled candidate of heat sink in thermal management applications. The inappropriate thermal interface material (TIM), however, could severely restrain the application of GF as heat sink. In this study, GF heat sink was assembled with SAC305 (Sn-3.0Ag-0.5Cu, wt. %) solder through ultrasonic-assisted soldering approach. Due to ultrasonic effects, the soldered interface for heat transfer exhibited compact structure. The forming of Ag_3Sn and Cu_6Sn_5 nanoparticles at interface could improve the interfacial coefficient gradient of thermal expansion. Comparing to traditional thermally conducted packaging method, soldering-assembled GF heat sinks exhibited excellent cooling efficiency, which could be maintained after more than 50 thermal cycles from 0 to 100 °C, and after thermal aging treatments for over 48 h under 150 °C in air. In the mechanical performance tests, the ultrasonic-assisted soldered GF joints showed high structural stability. These findings reinforce the significant potential of ultrasonic-assisted soldered GFs in thermal management.

Keywords Graphite films · Ultrasonic-assisted soldering · Thermally conducted interface · Thermal interface materials · Thermal management

1 Introduction

Due to the miniaturized and integrated design of electronic devices, the power levels escalate constantly, which in turn generate more heat flux [1, 2]. Thus, thermal management has become the main challenge towards the development in electronic industry. Employing heat sinks with prominent thermal conductivity and ensuring effective heat transfer from heat elements to heat sinks are two crucial tasks that need to be solved [3–5]. Unique properties of graphite film (GF), including ultrahigh thermal conductivity, light weight, and excellent corrosive resistivity, have made GF an unrivaled candidate as heat sink in next-generation thermal management applications [6–8]. However, the utilization of inappropriate thermal interface materials (TIMs) can severely restrict the integrated performance of GF heat sinks [9].

TIM is defined as the material applied at the interface between two components such as heating element and heat sink, to guarantee effective heat transfer [4]. In practical applications, the asperities of two solid surfaces can greatly reduce thermal coupling due to poor thermal conductivity of the air inside interfacial gaps [10]. Consequently, TIMs with relatively high thermal conductivity compared with air are employed as an effective heat conduction path at interfaces [11]. Generally, TIMs can be classified into three categories including polymer-based TIMs, carbon-based TIMs, and low melting solders [4]. Polymer-based TIMs are the most widely used TIMs, containing thermal greases, thermally conductive adhesives, thermally plastic materials, and so on. These materials, however, exhibit low thermal conductivity [1] (< 10 W m^{-1} K^{-1} in general), poor resistance to oxidation, and aging [12, 13]. Carbon-based TIMs including diamond films [14], vertical-aligned carbon nanotube (CNT) films [15], and vertical graphene arrays [16] exhibit good thermal conductivity. However, the non-deformability of carbon-based TIMs under pressure (mechanical joining) makes them difficult to fill the micro-gaps, which may create higher interfacial thermal resistance. Notably, low-melting solders with excellent deformability

✉ Yong Xiao
yongxiao@whut.edu.cn

✉ Daping He
hedaping@whut.edu.cn

1 School of Materials Science and Engineering, Wuhan University of Technology, Wuhan 430070, China

2 Hubei Engineering Research Center of RF-Microwave Technology and Application, School of Science, Wuhan University of Technology, Wuhan 430070, China

3 State Key Laboratory of Silicate Materials for Architectures, Wuhan University of Technology, Wuhan 430070, China

Published online: 22 April 2021

can serve as efficient TIMs with high thermal conductivity and low thermal interface resistance down to 50 $mm^2\ K\ W^{-1}$ [17]. Furthermore, soldering of components can achieve metallurgical connection at atomic scale, which displays high structural stability [18]. Hence, low-melting solders are regarded as promising TIMs for the application of GF as heat sinks.

Unfortunately, wetting issue of low-melting solders [19] on rough GF surface [20] can create high interfacial thermal resistance and structural instability. To address this challenge, many approaches have been proposed to modify GF surface for improved wettability, including vacuum evaporation plating [21], magnetron sputtering [22], chemical vapor infiltration [23], chemical plating [24], sintering [25], etc. Nevertheless, the modified layer containing active elements presents strong inclination of oxidation in air, which may create pore interface. Besides, interfacial wreck induced by thermal shock during heat dissipating resulted from mismatch of coefficient of thermal expansion (CTE) between GF [26] and solders [27] may lead to plunge of cooling efficiency and structural failure of the thermally conducted joints. Therefore, it is still challenging to employ low-melting solders as TIMs during assembling of efficient GF heat sinks.

In our previous research [28], we have reported ultrasonic-assisted soldering technique for micro joining of graphene-assembled films, which exhibited excellent electrical properties. But the application of this technique in GF heat sinks still requires further verification. Simultaneously, the CTE mismatch between amorphous carbon (a-C) layer and pure Sn solder remained large, considering the frequent thermal shocks and thermal cycles during thermal dissipating process; it is urgent to improve CTE gradient of interfacial structure.

Herein, by adopting ultrasonic-assisted soldering technique, we successfully employed SAC305 (Sn-3.0Ag-0.5Cu, wt. %) solders as TIM to realize assembling of GF heat sinks. Due to degasification and cavitation effects of ultrasonic waves, the soldered interface inside thermally conducted joints of GF exhibits no interfacial defects such as nanogaps or cracks. Besides, Ag_3Sn and Cu_6Sn_5 nanoparticles formed at SAC305/amorphous carbon (a-C) interface are supposed to help improve the interfacial CTE gradient. In consequence, GF heat sink employing SAC305 as TIMs can maintain superior cooling efficiency after numerous thermal cycles and thermal aging treatments. In addition, the ultrasonically soldered GF joints are demonstrated to have high structural stability which is of great importance in practical applications of thermal management.

2 Materials and methods

2.1 Materials

Polyimide films were purchased from Nanjing Fante Plastic Industry Co., Ltd. SAC305 solder was purchased from Shenzhen Jushi Electronics Co., Ltd. Aluminum (Al) block was purchased from Shanghai Jiashi Metal Products Co., Ltd. The silver paste (SP, DOUBLEBOND CHEMICAL DB2013), copper (Cu) foil, and aluminum (Al) foil were all purchased from Wuxi Chengyi Education Technology Co., Ltd. The ceramic heaters were purchased from Shenzhen Xinghe Electronic Co., Ltd.

2.2 Preparation of GF

Firstly, the polyimide precursor was heated to 1300 °C at a heating rate of 2 °C/min and held for 5 h in a vacuum furnace (CX-GFL-R20/30) to carbonize. Secondly, the obtained film was graphitized in the furnace by sintering at 2850 °C for 2 h; the heating rate from 1300 to 2850 °C was 5 °C /min. Thirdly, the furnace with GF inside was cooled down to room temperature naturally. Significantly, the above three procedures were all operated under argon (Ar) atmosphere. In the end, the GF with a thickness of 25 μm was obtained by rolling process and cut into a size of 100 mm × 10 mm by laser cutting in a laser cutting machine (LPKF ProtoLaser S).

2.3 Ultrasonic-assisted soldering process of GF

At first, GF was dipped into molten SAC305 solder at 250 °C, with ultrasonic vibration for 20 s. Next, GF was turned over and ultrasonically dipped for 20 s again. Then, GF with SAC305 coatings was obtained, and the ultrasonic-assisted soldering of GF was realized by remelting the SAC305 coatings on GF between two Al blocks.

2.4 Thermal cycles and thermal aging treatments of GF heat sinks

One thermal cycle of GF heat sinks referred to that device was held at 100 °C for 5 min, and then placed at 0 °C (mixtures containing ice and water) for 5 min. And thermal aging treatment was performed at 150 °C in air.

2.5 Characterizations and measurements

The morphology and interfacial structure of GFs, SAC305 coatings, and GF soldered joints were investigated by SEM (JSM-7610F Plus), XRD (Rigaku Smartlab, Cu Kα, λ = 1.5406 Å), Raman spectrum (Spectra-Physics Model 2025 argon ion laser, λ = 457.9 nm), 3D microscope with ultra-depth field (KEYENCE VH-Z500R), and TEM (Titan G2 60-300). TEM samples were prepared by the focus ion beam system (Nova NanoSEM 450). In addition, the tensile test

was carried out in the electromechanical universal testing machine (MTS E44.104, 0.1 mm/min), and the shear test was conducted in a micro-mechanical tester (Instron5848, 1 mm/min).

3 Results and discussion

Figure 1a displays the photograph of commercial GF, which was manufactured by high-temperature annealing and rolling of polyimide precursor. As displayed in Fig. 1b, compared with traditional thermally conducted materials such as Cu and Al, GF can keep structural stability after repeated bending. Besides, GF exhibits excellent thermal conductivity (1273.8 W m^{-1} K^{-1}, Table S1 in Supplementary materials) and light weight (Fig. 1c). Therefore, GF is regarded as a promising candidate as light heat sink in efficient thermal management system. As depicted in Fig. 1d, a sharp and strong peak of C (002) at around 2θ = 26.55° can be observed in the X-ray diffraction (XRD) pattern of GF, indicating that the interlayer spacing of GF is about 0.335 nm according to Bragg equation. Meanwhile, the sharp peak of C (004) revealed the high graphitization degree of GF. Besides, the inset in Fig. 1d is the Raman spectrum of GF. The dropping intensity ratio of D band and G band (I_D/I_G) is 0.075, manifesting that the GF exhibits less defects and high graphitization degree, because D band (1350 cm^{-1}) is caused by defect-induced breathing mode, and G band (1581 cm^{-1}) is the symbol of high crystalline graphite [29, 30]. Generally, defect plays a major role in affecting the thermal conductivity of GF [6]. Figure 1e shows the cross-sectional scanning electron microscopy (SEM) images of GF, indicating that the GF is composed of highly oriented stacking structure of graphene multilayers with a thickness of 25 μm. Figure 1f is the surface picture of GF taken by a 3D microscope with ultra-depth field. A mass of wrinkles and pits can be observed on GF surface. Such rough surface may trap airs and lead to forming of structural defects such as nanocavities and microcracks at GF/TIM interface, which can generate high thermal resistance at interface and reduce heat dissipating efficiency [1, 4].

SAC305 is one of the most widely used commercial low-melting solders, which is considered as a promising TIM candidate in thermal management applications due to its excellent thermal conductivity and high deformability [9, 31]. However, the wetting issue of SAC305 on GF surface hinders its application as TIM. In our philosophy, ultrasonic-assisted soldering technique was utilized to promote

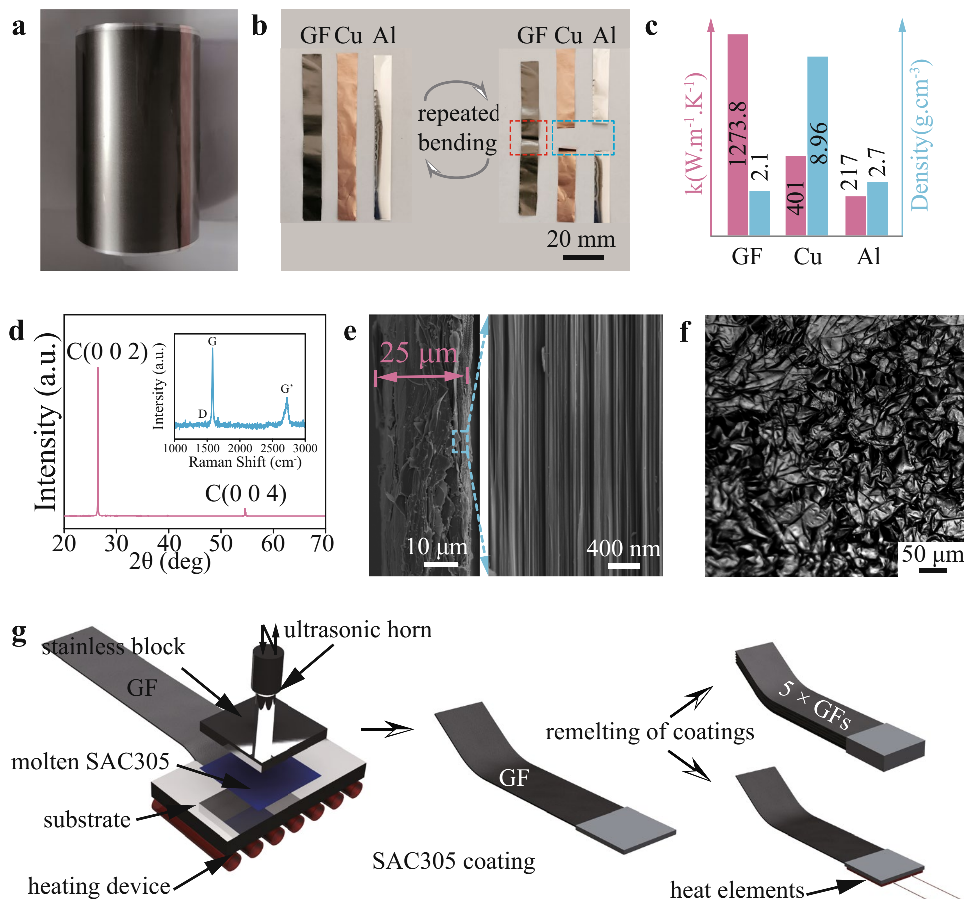

Fig. 1 **a** Photograph of commercial GF product. **b** Flexibility comparison among GF, Cu, and Al. **c** A histogram showing thermal conductivity and density of GF, Cu, and Al, respectively. **d** XRD pattern of GF, the inset is the Raman spectrum of GF. **e** Cross-sectional SEM images of GF. **f** Surface picture of GF taken by a 3D microscope with ultra-depth field. **g** Schematic diagram illustrating the prepared process of SAC305 coatings on GF, and soldering process of multiple GFs

the wettability of SAC305 solder. Figure 1g schematically illustrates the preparation process of SAC305 coatings on GF surface with ultrasonic assistance and the soldering process of multilayer GFs. After ultrasonically dipping process, neat SAC305 coatings can be quickly prepared within 40 s on GF surface (Fig. 2a). Subsequently, GF with SAC305 coatings can be easily soldered with other components by remelting the coatings.

Interfacial combination plays the vital part in connection performance, especially in heat-conducted performance [4]. However, the wrinkle structure on GF surface may trap air and then introduce structural defects into bonding interface, which can be exacerbated especially when SAC305 performs poor wettability on GF surface. Figure 2b shows the cross-sectional SEM image of GF with SAC305 coatings. Results show that the ultrasonically prepared SAC305 coatings exhibit a uniform thickness of 50 μm on GF surface. Significantly, no structural defects (such as micro-cavities, interfacial cracks, etc.) were observed inside the coatings and at the bonding interface of GF/SAC305 (Fig. 2c). Figure 2d is the cross-sectional image of 5-layer GF-soldered joints. The thickness of the soldered joints was adjusted to 200 μm by applying pressure during remelting process. As shown in Fig. 2e, the GF/SAC305 interface after remelting process exhibits no structural defects inside the SAC305 region or at the interface, indicating that the compact-soldered interface between GF and SAC305 coatings can sustain the remelting process of SAC305 coatings.

Figure 2f presents the intensity distribution of different elements along two white lines at interface measured by energy dispersive spectrometer (EDS). The intensity of oxygen peak barely fluctuates at the interface, demonstrating that air trapped inside pits on GF surface were eliminated completely, which is beneficial to high-efficient heat conduction [4]. Air removal can be ascribed to the introduction of ultrasonic waves. Under ultrasonic vibrating, the induced cavitation bubbles can "gather" gas which was dissolved into liquid solder during growing [32], and the dissolved gas can be supplied by air which was trapped in rough interface of GF/liquid SAC305 [33]. Consequently, the air at interface is gradually sucked by acoustic bubbles. As cavitation bubble explodes, part of gas may dissolve into liquid solder to an equilibrium state, the residual gas may emerge from liquid solder and escape to ambient air [34, 35]. Furthermore, micro-jets and shock waves induced by explosion of bubbles may hit against GF surface [33], which may squeeze out the trapped air, and contribute to the wetting and the spreading of liquid SAC305 solders [36, 37].

Interestingly, segregation of Ag and Cu was observed at interface in Fig. 2f, which may be caused by prior nucleation growth of Ag_3Sn and Cu_6Sn_5 under high supercooling at interface [38, 39]. The interfacial supercooling may be resulted from high-temperature liquid SAC305 solder and solid GF with ultrahigh thermal conductivity [40]. Simultaneously, the bonding interface was analyzed by transmission electronic microscope (TEM). Figure 2g is the image of TEM sample prepared by focused ion beam thinning process. Figure 2h shows the scanning transmission electronic microscope (STEM) image and elemental distribution of the corresponding marked pink rectangle region measured by energy dispersive X-ray spectroscopy (EDX). Results show that nano-size Ag-rich and Cu-rich phases are distributed along interface and inside solder. It is notable that the distribution of O element is not segregated near GF/SAC305 interface, which is consistent with the result of EDS line scanning in Fig. 2f.

Figure 2i is the HRTEM image of GF/SAC305 interface. Obviously, no nano-defects were observed, which manifested that compact combination is formed at interface between GF and SAC305. The region with the lattice spacing of 0.34 nm is GF, while the region with the lattice spacing of 0.21 nm is probably Ag_3Sn phase according to EDX elemental mapping in Fig. 2h and XRD pattern of SAC305 solder (Fig. S1, Supplementary materials). Significantly, an amorphous layer with a thickness of 2 nm was observed at the bonding interface. Such a connection format of amorphous transition layer between metals and carbon-based materials has been reported frequently in previous studies. For instance, Liang et al. [41] reported an amorphous layer at Al/diamond interface, and Huang et al. [42] found that there was an amorphous layer at Al/graphite interface. Owning to ultralow thickness of amorphous layer, it is arduous to determine the accurate composition of the amorphous layer. Based on the ultrasonic-assisted soldering technology, the amorphous layer is considered as an amorphous carbon (a-C) layer, formed by the ultrasonic bombardment on GF surface, and the detailed formative process under the action of ultrasound was analyzed in our previous work [28].

According to Fig. 2h, i, the GF with a continuous a-C layer on surface may contact with SAC305 matrix by mixed Sn/a-C, Ag_3Sn/a-C, and Cu_6Sn_5/a-C interfaces. The CTE of Sn, Ag_3Sn, Cu_6Sn_5 are 22.0×10^{-6} m K^{-1}, 4.7×10^{-6} m K^{-1}, and 6.3×10^{-6} m K^{-1}, respectively [43], while the CTE of a-C layer is in the range of 1 to 8×10^{-6} m K^{-1} [26, 44]. Thus, compared with a-C/Sn interface reported previously, the formed Ag_3Sn and Cu_6Sn_5 at interface can enhance the matching degree of interfacial CTE. In other words, the interfacial structure between GF and SAC305 performs a smoother CTE gradient, which may be helpful to improve the resistance to thermal shocks and thermal cycles. Even though the thermal conductivity of a-C is as low as 1.6 W m^{-1} K^{-1} [26], the thermal dissipating ability of the entire system can maintain excellent due to ultrathin thickness of the a-C layer [42]. In addition, the soldered interface bonded by a-C has been verified to be mechanically stable [45]. Therefore, the thermal conduction joints of GFs prepared

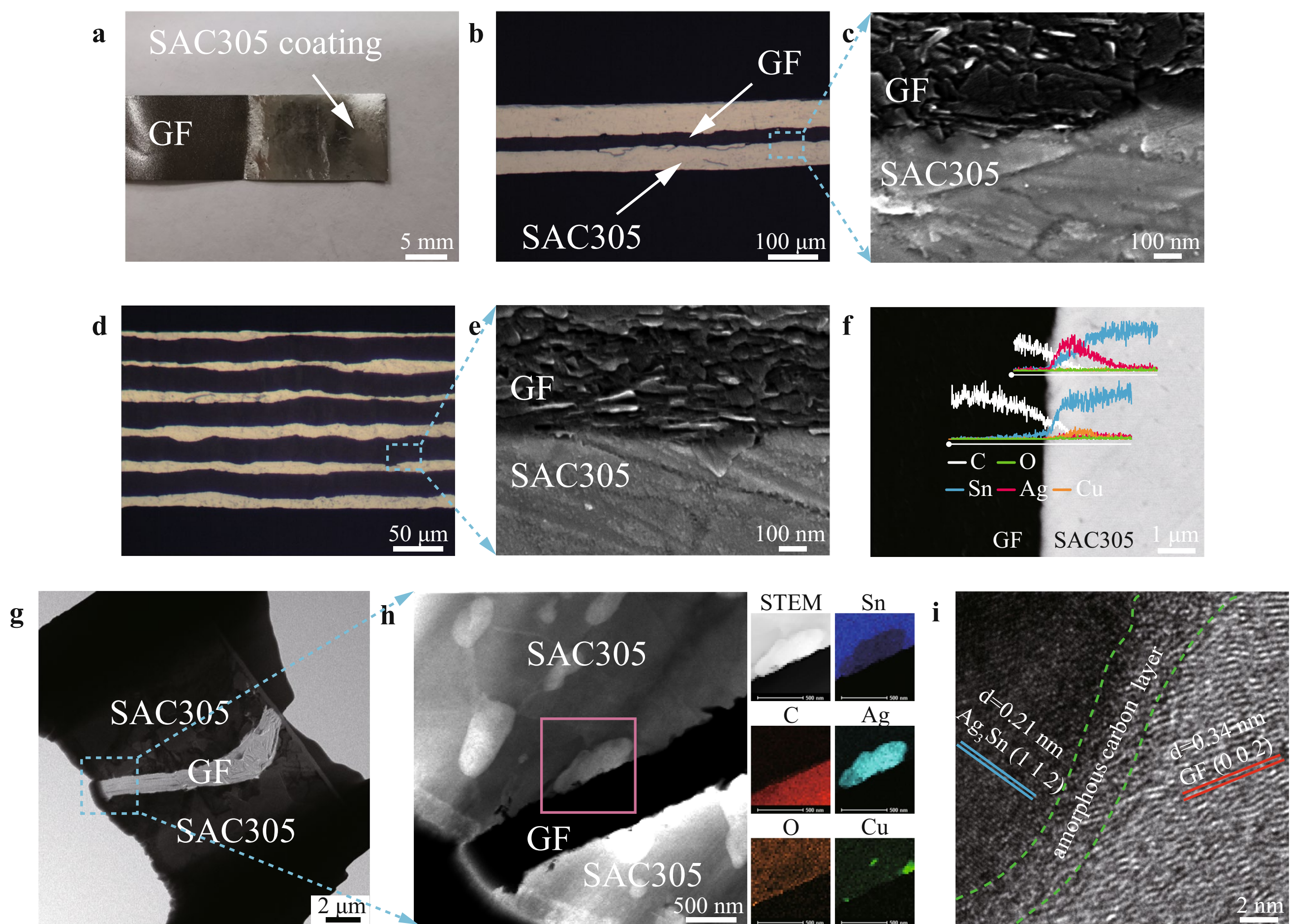

Fig. 2 **a** Photograph of SAC305 coating on GF surface prepared with ultrasonic assistance. **b**, **c** Cross-sectional SEM images of GF with a SAC305 coating. **d**, **e** Cross-sectional SEM images of 5-layer GFs soldered joint prepared by remelting SAC305 coatings on GF surface. **f** Intensities distribution of different elements along two white lines at GF/SAC305 interface measured by EDS. **g** Image of TEM sample prepared by focus ion beam thinning. **h** STEM image of GF/SAC305 interface and EDX elemental mappings of the marked pink rectangle region. **i** High-resolution TEM image of GF/SAC305 interface

with ultrasonic assistance may present durably satisfactory thermal dissipating performance and mechanical property.

Figure 3a displays the traditional thermal management system containing a heating element, a layer of TIM, and a heat sink. Traditionally, heat sink is composed of rigid Al or Cu block with fin structure, and TIM is usually thermal conducted silicon grease. In this study, we employed GF as heat sink and utilized SAC305 solder as TIM with ultrasonic-assisted soldering method, to realize advanced thermal management. To evaluate the potential of GF heat sinks assembled by different TIMs, a system was designed to investigate heat transfer in electronic components (Fig. 3b, Fig. S2 in Supplementary materials). GF and Cu foil (heat sinks, 100 mm × 10 mm × 25 μm) were mounted to a ceramic heater (heating element, 10 mm × 10 mm × 1 mm) with a heating power of 1 W by employing different TIMs. Besides, surface temperatures of ceramic heaters were monitored and recorded by commercial K-thermocouple wires.

Figure 3c is the plot of temperature versus time, showing the heat transfer efficiency of different combinations of heat sink and TIM. Under room temperature which was kept to be 20 °C, surface temperatures of ceramic heaters corresponding to various heat sinks and TIMs stabilized after 500 s. Hence, the heat dissipating ability can be investigated by comparing the equilibrium temperature after heating for 500 s. As shown in Fig. 3c, the equilibrium temperature of the ceramic heater connected with a piece of Cu foil by press fit reached 90.2 °C. By only replacing the Cu foil with GF, the equilibrium temperature dropped to 77.3 °C, demonstrating the superiority of GF as heat sink. Moreover, the equilibrium temperature of the ceramic heater bonded with a piece of GF by SP was 3.1 °C lower than that of ceramic heater connected by press fit. When heat was transferred from heating elements to heat sinks without employing TIMs, interfacial gaps with air trapped inside would generate high thermal resistance due to extremely low thermal conductivity of air

(as low as 0.024 W m K^{-1} at room temperature [46]). Hence, the lower equilibrium temperature of heater bonded by SP can be attributed to the filling of interfacial gaps by TIMs as shown in the inset of Fig. 3c. Notably, the equilibrium temperature of the ceramic heater soldered ultrasonically with a piece of GF can further drop to 71.7 °C, showing better thermal dissipating efficiency than that of the heater bonded by SP. Furthermore, the ultrasonic-assisted soldering of 5 pieces of GF exhibited excellent thermal transfer ability, which can keep the temperature of ceramic heater below 52.5 °C. It is worthwhile to notice that the weight of 5 pieces of GF is equal to a piece of Cu foil with the same thickness. The excellent thermal dissipating efficiency of GF heat sinks assembled by ultrasonic-assisted soldering should be attributed to the excellent thermal conductivity of GF and SAC305 solder, coupled with the low interfacial thermal resistance of compact interface [9, 17].

As shown in Fig. 3d, e, the equilibrium temperature of ceramic heater ultrasonically soldered with 5 pieces of GF can remain stable after multiple severe thermal cycles and thermal aging treatments (detailed experimental parameters are included in Experimental Section), indicating that compared with traditional polymer-based TIMs [9, 47], thermally conducted joints of GFs assembled with SAC305 solder by ultrasonic-assisted soldering can provide long-term and durably superior service in thermal management system.

Apart from high thermal dissipating efficiency, the assembly of heat sinks should meet the requirement of high structural stability. Figure 4a shows a typical GF soldered joint prepared by remelting the SAC305 coatings on GFs

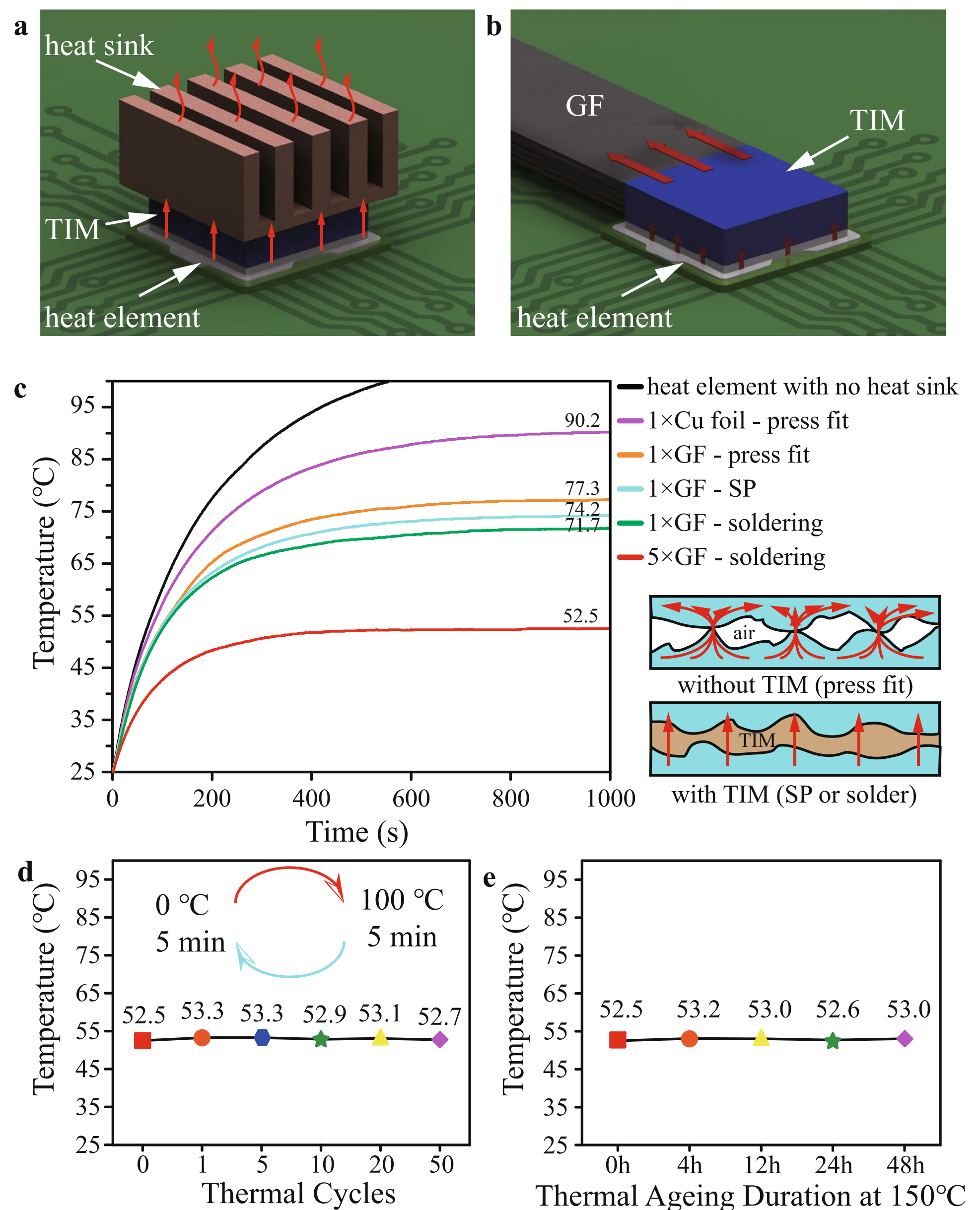

Fig. 3 Thermal dissipating performance of GF heat sinks assembled by different TIMs. **a** Schematic of traditional thermal management system containing a chip (heating element), a layer of TIM and a heat sink. **b** Schematic diagram showing the test system of thermal dissipating ability of GF heat sink using different TIMs. The heat element is a ceramic heater with a heating power of 1 W (5 V, 0.2 A). **c** Plot of temperature versus time showing the heat transfer efficiency of heat sinks using different TIMs (more details can be seen in Supplementary materials). The inset in **c** shows the different interface with TIM (press fit) and without TIM (connected by SP or solder). **d** Equilibrium temperature evolution of the ceramic heater employing the heat sink assembled by ultrasonic-assisted soldering of 5-layer GFs after multiple thermal cycles and **e** thermal aging treatment at 150 °C

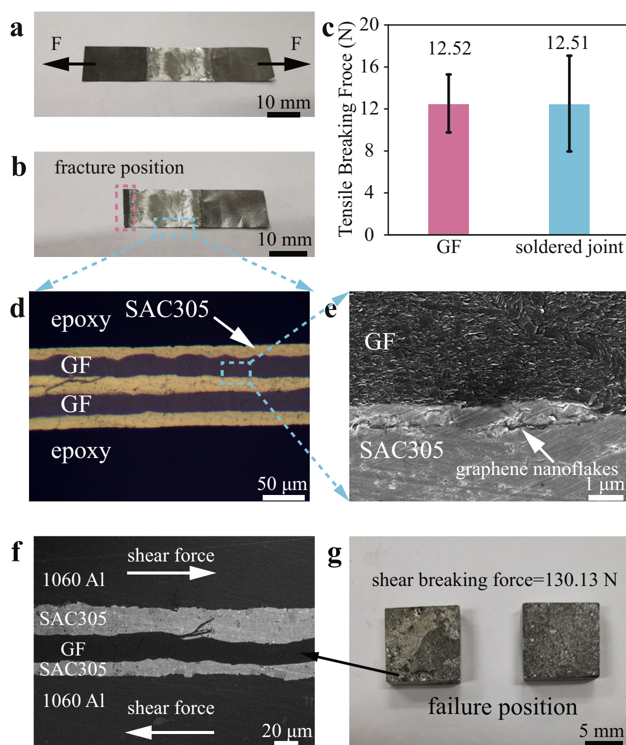

Fig. 4 Mechanical performance tests. **a** Photograph of a typical GF-soldered joint. **b** Photograph of the failed GF-soldered joint after tensile test. **c** Comparisons of average tensile breaking force between GFs and GF-soldered joints. **d**, **e** Cross-sectional SEM images of the failed GF-soldered joint in **b**. **f** Cross-sectional SEM image of a typical Al-SAC305-GF-soldered joint. **g** Photograph of the failed Al-SAC305-GF-soldered joint after shear test

surface, in which each piece of GF was cut into the size of 10 mm × 30 mm, and the overlapping area is 10 mm × 10 mm. Figure 4b displays the failed GF-soldered joints under tensile load. Notably, only the outer GF to the left of the GF-soldered joint was fractured, suggesting that the tensile resistance of GF-soldered joints was higher than that of GF. Figure 4c shows that the average tensile load of GFs and GF soldered joints when breaking. The average tensile breaking force of GF was 12.52 N, while that of GF-soldered joints was 12.51 N. As illustrated in Fig. 4d, e, the inner GF and bonding interface remain undamaged and intact, which demonstrate that the GF-soldered joints are of high structural stability to allow the tensile loading.

Taking account of the lapped structure of GF heat sinks on heating elements, and the poor bonding force between GF interlayers [48], shear resistance of GF heat sinks should be analyzed. Hence, we fabricated the Al-SAC305-GF-soldered joints with the overlapping area of 10 mm × 10 mm as shown in Fig. 4f (fabrication procedure of Al-SAC305-GF-soldered joints is shown in Fig. S3, Supplementary materials). Shear test of the Al-SAC305-GF-soldered joints was carried out according to Fig. S4 in Supplementary materials, to simulate GF heat sinks under shear load. Figure 4g shows the failed Al-SAC305-GF joint after shear test. The fracture position under shear load was located in GF interlayer. Moreover, the average shear load of Al-SAC305-GF joint when breaking was 130.14 N, which is much higher than the tensile breaking force of GF in this size. Thus, it can be concluded that the ultrasonic-assisted soldering of GF exhibits high structural stability, which can meet the requirement for the application in thermal management.

4 Conclusion

In conclusion, we developed an ultrasonic-assisted soldering approach to employ SAC305 solders as TIM for the assembling of GF heat sinks. Inside GF-soldered joints, the compact thermally conducted interface is obtained due to degasification and cavitation effects induced by ultrasonic waves. Besides, the formation of Ag_3Sn and Cu_6Sn_5 nanoparticles at SAC305/a-C interface can enhance CTE matching degree at the thermally conducted interface. As a consequence, GF heat sinks assembled by the TIM of SAC305 solder show superior thermal dissipating efficiency compared to traditional thermally conductive adhesives, and the excellent thermal dissipating efficiency is demonstrated to be stable after multiple thermal cycles and thermal aging treatments. Moreover, the thermally conducted joints of GF prepared with ultrasonic assistance exhibit high structural stability, indicating its great practical potential in thermal management.

Supplementary information The online version contains supplementary material available at https://doi.org/10.1007/s42114-021-00255-8.

Acknowledgements The authors thank Prof. Zhi Zhang from Huazhong University of Science and Technology for the TEM characterization of interface structure. The authors thank Dr. Xiaoqing Liu from Center for Materials Research and Analysis of Wuhan University of Technology for the data analysis of TEM.

Author contribution Y. X. and D. H. conceived the project. H. F., Y. X., and D. L. designed and performed the ultrasonic-assisted soldering of graphite films. H. F., P. L., and W. Q. performed the characterizations and carried out the mechanical performance test. H. F. carried out the test on thermal dissipating performance of GF heat sink using different TIMs. H. F. wrote the paper. Y. X., X. Z., and D. H. revised the paper.

Funding This study was funded by National Natural Science Foundation of China (No. 51605357) and 2018 National Key R&D Program of China 257.

Availability of data and material All data generated or analyzed during this study are included in this published article and its supplementary information files.

Declarations

Competing interests The authors declare no competing interests.

References

1. Song H, Liu J, Liu B, Wu J, Cheng HM, Kang F (2018) Two-dimensional materials for thermal management applications. Joule 2:442–463. https://doi.org/10.1016/j.joule.2018.01.006
2. Moore AL, Li S (2014) Emerging challenges and materials for thermal management of electronics. Mater Today 17:163–174. https://doi.org/10.1016/j.mattod.2014.04.003
3. Deng Y, Liu J (2010) A liquid metal cooling system for the thermal management of high power LEDs. Int Commun Heat Mass Transf 37:788–791. https://doi.org/10.1016/j.icheatmasstransfer.2010.04.011
4. Razeeb KM, Dalton E, Cross GLW, Robinson AJ (2018) Present and future thermal interface materials for electronic devices. Int Mater Rev 63:1–21. https://doi.org/10.1080/09506608.2017.1296605
5. Liu Y, Chen HF, Zhang HW, Li YX (2015) Heat transfer performance of lotus-type porous copper heat sink with liquid GaInSn coolant. Int J Heat Mass Transf 80:605–613. https://doi.org/10.1016/j.ijheatmasstransfer.2014.09.058
6. Peng L, Xu Z, Liu Z, Guo Y, Li P, Gao C (2017) Ultrahigh thermal conductive yet superflexible graphene films. Adv Mater 29:1700589. https://doi.org/10.1002/adma.201700589
7. Akbari A, Cunning BV, Joshi SR, Wang C, Camacho-Mojica DC, Chatterjee S, Modepalli V, Cahoon C, Bielawski CW, Bakharev P, Kim GH, Ruoff RS (2020) Highly ordered and dense thermally conductive graphitic films from a graphene oxide/reduced graphene oxide mixture. Matter 2:1198–1206. https://doi.org/10.1016/j.matt.2020.02.014
8. Xin G, Sun H, Hu T, Fard HR, Sun X, Koratkar N, Borca-Tasciuc T, Lian J (2014) Large-area freestanding graphene paper for superior thermal management. Adv Mater 26:4521–4526. https://doi.org/10.1002/adma.201400951
9. Liou B-H, Chen C-M, Horng R-H, Chiang Y-C, Wuu D-S (2012) Improvement of thermal management of high-power GaN-based light-emitting diodes. Microelectron Reliab 52:861–865. https://doi.org/10.1016/j.microrel.2011.04.002
10. Prasher RS, Koning P, Shipley J, Devpura A (2003) Dependence of thermal conductivity and mechanical rigidity of particle-laden polymeric thermal interface material on particle volume fraction. J Electron Packag Trans ASME 125:386–391. https://doi.org/10.1115/1.1602703
11. Xu J, Munari A, Dalton E, Mathewson A, Razeeb KM (2009) Silver nanowire array-polymer composite as thermal interface material. J Appl Phys 106:1–8. https://doi.org/10.1063/1.3271149
12. Bockenheimer C, Fata D, Possart W (2004) New aspects of aging in epoxy networks. I. Thermal aging. J Appl Polym Sci 91:361–368. https://doi.org/10.1002/app.13092
13. Zahra Y, Djouani F, Fayolle B, Kuntz M, Verdu J (2014) Thermo-oxidative aging of epoxy coating systems. Prog Org Coatings 77:380–387. https://doi.org/10.1016/j.porgcoat.2013.10.011
14. Hsu CY, Lin YL (2013) Thermal characteristics of high-power LED packages with dissipation film. Appl Mech Mater 397–400:1767–1771. https://doi.org/10.4028/www.scientific.net/AMM.397-400.1767
15. Ganguli S, Roy AK, Wheeler R, Varshney V, Du F, Dai L (2013) Superior thermal interface via vertically aligned carbon nanotubes grown on graphite foils. J Mater Res 28:933–939. https://doi.org/10.1557/jmr.2012.401
16. Xu S, Wang S, Chen Z, Sun Y, Gao Z, Zhang H, Zhang J (2020) Electric-field-assisted growth of vertical graphene arrays and the application in thermal interface materials. Adv Funct Mater 2003302:1–7. https://doi.org/10.1002/adfm.202003302
17. Barako MT, Gao Y, Marconnet AM, Asheghi M, Goodson KE (2012) Solder-bonded carbon nanotube thermal interface materials. In: 13th InterSociety Conference on Thermal and Thermomechanical Phenomena in Electronic Systems. IEEE, pp 1225–1233
18. Tuan WH, Chou TT, Kao CT, Wang SY, Weng BJ (2018) Thermal diffusivity of graphite paper and its joint with alumina substrate. J Eur Ceram Soc 38:187–191. https://doi.org/10.1016/j.jeurceramsoc.2017.07.029
19. Sánchez SA, Narciso J, Louis E, Rodríguez-Reinoso F, Saiz E, Tomsia A (2008) Wetting and capillarity in the Sn/graphite system. Mater Sci Eng A 495:187–191. https://doi.org/10.1016/j.msea.2007.09.090
20. Wang Z, Li P, Song R, Qian W, Zhou H, Wang Q, Wang Y, Zeng X, Ren L, Yan S, Mu S, He D (2020) High conductive graphene assembled films with porous micro-structure for freestanding and ultra-low power strain sensors. Sci Bull 65:1363–1370. https://doi.org/10.1016/j.scib.2020.05.002
21. Peacock MA, Roy CK, Hamilton MC, Wayne Johnson R, Knight RW, Harris DK (2016) Characterization of transferred vertically aligned carbon nanotubes arrays as thermal interface materials. Int J Heat Mass Transf 97:94–100. https://doi.org/10.1016/j.ijheatmasstransfer.2016.01.071
22. Moutis NV, Jimenez C, Azpiroz X, Speliotis T, Wilhelmi C, Messoloras S, Mergia K (2010) Brazing of carbon-carbon composites to Nimonic alloys. J Mater Sci 45:74–81. https://doi.org/10.1007/s10853-009-3893-x
23. Chang J, Zhang Q, Lin Y, Shao P, Pei Y, Zhong S, Wu G (2019) Thermal management applied laminar composites with SiC nanowires enhanced interface bonding strength and thermal conductivity. Nanoscale 11:15836–15845. https://doi.org/10.1039/c9nr04644e
24. Zhao S, Zheng Z, Huang Z, Dong S, Luo P, Zhang Z, Wang Y (2016) Cu matrix composites reinforced with aligned carbon nanotubes: mechanical, electrical and thermal properties. Mater Sci Eng A 675:82–91. https://doi.org/10.1016/j.msea.2016.08.044
25. Fu W, Hu SP, Song XG, Li JX, Cao J, Feng JC, Wang GD (2017) Wettability and bonding of graphite by Sn0.3Ag0.7Cu-Ti alloys. Carbon 121:536–543. https://doi.org/10.1016/j.carbon.2017.06.030
26. Amaratunga GAJ, Andrienko I, Anguita JV, Aono M, Arnold W, Barklie RC, Beghi MG, Bilek MM, Bottani CE (2003) Properties of Amorphous Carbon, 29th edn. The Institution of Electrical Engineers, London
27. Tollefsen TA, Larsson A, Løvvik OM, Aasmundtveit K (2012) Au-Sn SLID bonding—properties and possibilities. Metall Mater Trans B 43:397–405. https://doi.org/10.1007/s11663-011-9609-z
28. Fu H, Xiao Y, Song R, Wang Z, Ji H, He D (2020) Rapid soldering of flexible graphene assembled films at low temperature in air with ultrasonic assistance. Carbon 158:55–62. https://doi.org/10.1016/j.carbon.2019.11.089
29. Caņado LG, Takai K, Enoki T, Endo M, Kim YA, Mizusaki H, Jorio A, Coelho LN, Magalhães-Paniago R, Pimenta MA (2006) General equation for the determination of the crystallite size la of nanographite by Raman spectroscopy. Appl Phys Lett 88:1–4. https://doi.org/10.1063/1.2196057
30. Reich S, Thomsen C (2004) Raman spectroscopy of graphite. Philos Trans R Soc London Ser A Math Phys Eng Sci 362:2271–2288
31. Mukhtar MFM, Abas A, Haslinda M, Ani FC, Abdullah MZ, Jalar A, Ismail R (2018) Discrete Phase Model (DPM) study of nano-reinforced Lead Free Solder Sn-3.0Ag-0.5Cu (SAC305). IOP Conf Ser Mater Sci Eng 370:012067. https://doi.org/10.1088/1757-899X/370/1/012067
32. Suslick KS (1989) The chemical effects of ultrasound. Sci Am 80–86. https://www.jstor.org/stable/24987145
33. Shchukin DG, Skorb E, Belova V, Möhwald H (2011) Ultrasonic cavitation at solid surfaces. Adv Mater 23:1922–1934. https://doi.org/10.1002/adma.201004494
34. Eskin DG (2015) Ultrasonic degassing of liquids. In: Power Ultrasonics. Elsevier, pp 611–631

35. Eskin G (1995) Cavitation mechanism of ultrasonic melt degassing. Ultrason Sonochem 2:S137–S141. https://doi.org/10.1016/1350-4177(95)00020-7
36. Yu WY, Liu SH, Liu XY, Shao JL, Liu MP (2015) Wetting behavior in ultrasonic vibration-assisted brazing of aluminum to graphite using Sn-Ag-Ti active solder. Surf Rev Lett 22:1–9. https://doi.org/10.1142/S0218625X15500353
37. Yu W, Liu Y, Liu X (2018) Spreading of Sn-Ag-Ti and Sn-Ag-Ti(-Al) solder droplets on the surface of porous graphite through ultrasonic vibration. Mater Des 150:9–16. https://doi.org/10.1016/j.matdes.2018.04.028
38. Li JF, Agyakwa PA, Johnson CM (2010) Kinetics of Ag3Sn growth in Ag–Sn–Ag system during transient liquid phase soldering process. Acta Mater 58:3429–3443. https://doi.org/10.1016/j.actamat.2010.02.018
39. Li JF, Agyakwa PA, Johnson CM (2011) Interfacial reaction in Cu/Sn/Cu system during the transient liquid phase soldering process. Acta Mater 59:1198–1211. https://doi.org/10.1016/j.actamat.2010.10.053
40. Ma Y, Li X, Zhou W, Yang L, Wu P (2017) Reinforcement of graphene nanosheets on the microstructure and properties of Sn58Bi lead-free solder. Mater Des 113:264–272. https://doi.org/10.1016/j.matdes.2016.10.034
41. Liang J, Yamajo S, Kuball M, Shigekawa N (2019) Room-temperature direct bonding of diamond and Al. Scr Mater 159:58–61. https://doi.org/10.1016/j.scriptamat.2018.09.016
42. Huang Y, Ouyang Q, Guo Q, Guo X, Zhang G, Zhang D (2016) Graphite film/aluminum laminate composites with ultrahigh thermal conductivity for thermal management applications. Mater Des 90:508–515. https://doi.org/10.1016/j.matdes.2015.10.146
43. Billah MM, Siddiquee RI, Motalab M (2019) Temperature dependent mechanical properties of inter-metallic compounds in nano-solder joints. In: AIP Conference Proceedings, p 140014
44. Yoon D, Son Y-W, Cheong H (2011) Negative thermal expansion coefficient of graphene measured by Raman spectroscopy. Nano Lett 11:3227–3231. https://doi.org/10.1021/nl201488g
45. Wang MS, Wang JY, Chen Q, Peng L-M (2005) Fabrication and electrical and mechanical properties of carbon nanotube interconnections. Adv Funct Mater 15:1825–1831. https://doi.org/10.1002/adfm.200500215
46. Lindsay AL, Bromley LA (1950) Thermal conductivity of gas mixtures. Ind Eng Chem 42:1508–1511. https://doi.org/10.1021/ie50488a017
47. Suh D, Moon CM, Kim D, Baik S (2016) Ultrahigh thermal conductivity of interface materials by silver-functionalized carbon nanotube phonon conduits. Adv Mater 28:7220–7227. https://doi.org/10.1002/adma.201600642
48. Wang G, Dai Z, Wang Y, Tan P, Liu L, Xu Z, Wei Y, Huang R, Zhang Z (2017) Measuring interlayer shear stress in bilayer graphene. Phys Rev Lett 119:036101. https://doi.org/10.1103/physrevlett.119.036101

Publisher's Note Springer Nature remains neutral with regard to jurisdictional claims in published maps and institutional affiliations.